




Excess explosivity driven by melt inclusions during the 946 CE Plinian eruption of Baekdusan

Gi Bom Kim ¹, Shane J. Cronin ², Jong Ok Jeong³, Sun Young Go⁴, Youn Soo Lee⁵, Jiaqi Liu⁶ & Young Kwan Sohn ⁷✉

Melt inclusions readily rupture and form gas bubbles during explosive volcanic eruptions, but their role as a volcanic gas source remains enigmatic. Here, we examined a pumice texture generated by the instantaneous bursting of melt inclusions during the 946 CE Plinian eruption at Baekdusan. The burst produced non-sheared, super-vesicular (>80 vol.% voids) bubble pockets, occupying volume fractions of 6–24% within the Millennium gray pumice. The bubble pocket texture suggests that the melt inclusions acted as an additional volcanic gas source that increased the volume of the erupting magma at the moment of magma fragmentation. Two distinctive feldspar-glass assemblages of either sanidine-bearing trachyte or anorthoclase-bearing rhyolite in the bubble pockets indicate that the chemical bimodality of the hemisphere-scale, 946 CE Baekdusan tephra resulted from cryptic mixing of two magmas. The excess explosivity induced by the bursting melt inclusions should be considered when modeling eruption dynamics and assessing volcanic hazards, therefore having broad volcanological implications.

¹ Department of Geological Sciences, Pusan National University, Busan 46241, Republic of Korea. ² School of Environment, The University of Auckland, 92019 Auckland, New Zealand. ³ Central Instrument Facility, Gyeongsang National University, Jinju 52828, Republic of Korea. ⁴ Volcano Research Group, Korea Institute of Geoscience and Mineral Resources, Daejeon 34132, Republic of Korea. ⁵ Division of Environmental Sciences and Engineering, Pohang University of Science and Technology, Pohang 37673, Republic of Korea. ⁶ Key Laboratory of Cenozoic Geology and Environment, Institute of Geology and Geophysics, Chinese Academy of Sciences, Beijing 100029, China. ⁷ Department of Geology, Gyeongsang National University, Jinju 52828, Republic of Korea. ✉email: yksohn@gnu.ac.kr

The growth of magmatic gas bubbles increases the volume of the ascending magma, thereby accelerating the ascent of magmatic foams through conduits to drive explosive volcanic eruptions¹. In ascending magma, small volumes of the melt may be trapped within the crystals as inclusions. The host melt is spontaneously saturated with volatiles, exsolves gases, and then nucleates bubbles as decompression reaches a critical level^{2,3}. However, melt inclusions retain gases for longer periods, unless crystal seals are broken via the process of so-called decrepitation⁴. As melt inclusions are mechanically separated from the host melt by crystalline solids, their chemistry and the timing of volatile exsolution cannot be different from those of the host melt, causing bubble formation in multiple stages. However, the behavior and role of melt inclusions as a volcanic gas source in erupting magma have been poorly explored, despite the potential significance of this process in modulating eruption intensities^{4–7}.

Baekdusan (or Changbaishan in Chinese) Volcano is a Quaternary intraplate stratovolcano situated on the border between North Korea and China (128°05'E, 42°01'N). This volcano has produced a series of explosive eruptions culminating in one of its most explosive (VEI of 6.4–7.2)⁸ known events in 946 CE, known as the Millennium Eruption⁹. The Millennium Eruption produced the B-Tm (Baekdusan-Tomakomai) tephra, which is a hemispheric-scale tephra marker readily identifiable by its unique trachytic-rhyolitic compositional heterogeneity in glass shards^{10–12}. The heterogeneous glass shards in the tephra have been attributed to two consecutive eruptions of rhyolitic phase-1 and trachytic phase-2 magmas or mixing of them during the Millennium Eruption^{13–15}. Yet, the roles and interplay of the two magmas in driving the 946 CE eruptions at Baekdusan are not clearly understood. Based on zircon and Ra/Th isotope ages of the chemo-stratigraphic members of Millennium Eruption, researchers have envisaged that the coexisting subvolcanic rhyolite and trachyte magmas were mixed and overturned by the injection of latite magma^{15–17} or CO₂-rich fluid¹⁸.

In this study, we document a unique chemo-textural zonation structure, here named the bubble pocket, found in the proximal Millennium gray pumice. Based on the bubble pocket structure, we propose two-step bubble formation during the 946 CE Plinian eruption at Baekdusan and reassess the essential but overlooked role of melt inclusions as an additional volcanic gas source that can potentially enhance the volcanic explosivity.

Geological backgrounds

Previous studies of volcano-stratigraphy of Baekdusan show that the present 2750-m-high stratovolcanic edifice and the summit caldera were formed via three eruptive stages^{19–21}. The first stage is marked by basaltic effusive eruptions that formed the lower shield of the volcano since the early Pleistocene. The basaltic eruptions mostly originated from the central vent, identical to the location of the present caldera, as well as from circumferential fissures. The second stage is known as the cone-construction stage since c. 1.0 Ma. Trachyte and trachyandesite lavas and subsequent trachyte and comendite cones formed the summit of the volcano probably until c. 20 ka. Afterward, the eruptions on Baekdusan became more explosive and formed a thick pile of pumice-fall and pyroclastic density current (PDC) deposits around the ~5-km-wide summit caldera, Cheonji (Tianchi in Chinese).

Multiple alternations between trachyte and comendite eruptions have continued during the last 100 ka, indicating that a bimodal magma-feeding system is still operative under the volcano^{16,17}. According to the recently revised stratigraphy¹⁹, the summit of Baekdusan comprises two pumice-fall units originating respectively from the c. 50 ka BP Tianwenfeng (TWF) eruption and from 946 CE Millennium Eruption with an intervening (c.

8–4 ka BP) clastogenic Qixiangzhan (QXZ) lava flow event. Despite ongoing debates, the 946 CE Millennium Eruption is generally regarded to be the latest explosive event of Baekdusan. The event comprises two eruptive phases marked by the phase-1 gray alkali rhyolitic and the phase-2 black trachytic pumice deposits without apparent depositional hiatus in between^{12,14} (Fig. 1). The phase-1 gray rhyolitic pumice deposit appears to be subdivided into the lower light-colored pumice-fall and upper light- and dark-colored (mingled) pumice-fall and PDC deposits bearing abundant carbonized woods and banded pumice¹².

There exists an ongoing debate on the Millennium Eruption and post-Millennium eruptive scenario. Geochronologists, based on zircon ages¹⁷ and Ra/Th model ages¹⁶, ascribe the uppermost trachyte deposits to the eruptions at 1668 CE, 1702 CE and 1903 CE as suggested based on historical accounts²⁰. However, studies on the stratigraphic field relationships and chemo-texture of the Millennium pumice ascribe the latest trachyte events solely to the second phase of the 946 CE Millennium Eruption^{12,14,22–24}.

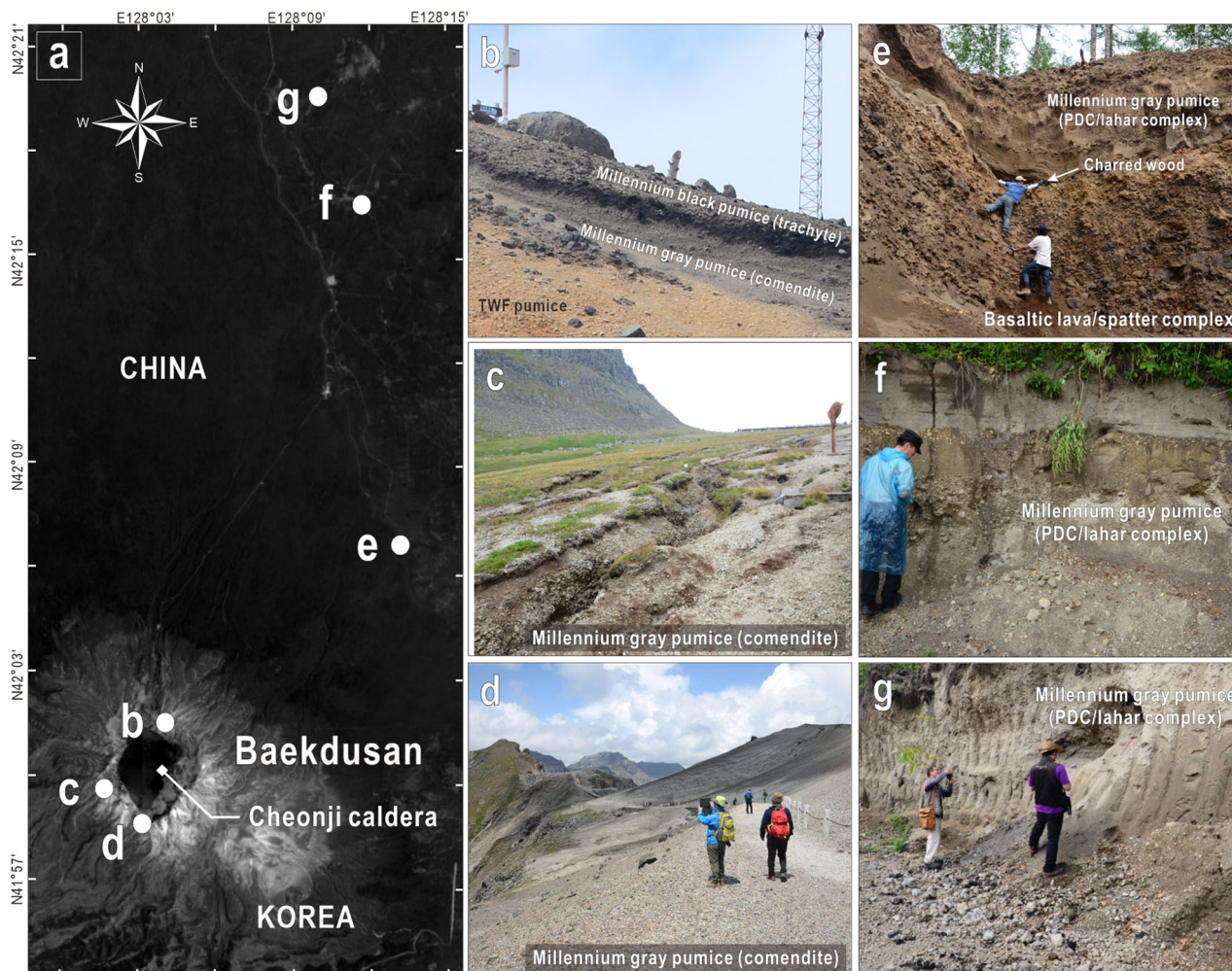
Investigation of zircon ages shows that the comendite that mainly fed the Millennium Eruption phase-1 was emplaced at the pre-eruptive storage level (~4 km below the volcano) around 12 ka by fractional crystallization from its parental magma at depth¹⁷. On the other hand, the trachyte magma that fed the Millennium Eruption phase-2 was emplaced much later roughly around 4–1 ka. As to the wide-range mixed zircon ages (2.6 ± 1.8 ka for autocrysts, 130 ± 10 ka and >230 ka for xenocrysts), it was inferred that the trachyte magma was derived from deeper parental trachytic mush oscillating around the zircon saturation level for a significant period of time (>200 ka). Based on Ra/Th model ages, it was suggested that from 2.5 to 1.5 ka, the trachyte magma accumulated adjacent to but isolated from the pre-existing comendite magma¹⁶.

The chemo-stratigraphy of the Millennium Eruption shows change in juvenile composition from (1) the earliest comendite to (2) the comendite-trachyte mingled and then (3) the trachyte with mingled comendite and finally (4) the trachyandesite or latite^{14,16,22}. It is inferred that the trachyandesite magma originating from a primitive basaltic source disturbed the stable separation, induced mixing between the comendite and trachyte magmas, and triggered the Millennium Eruption¹⁴. The continuous stratigraphic field relationship¹², apparent mingling texture and concordant Ra/Th model ages among different types of Millennium pumice¹⁶ support that mixing between trachyte and comendite magmas might have triggered the Millennium Eruption.

On the summit caldera of Baekdusan, the proximal air-fall pumice generated from the Millennium Eruption shows a sharp vertical transition in color and bulk rock chemistry from the climactic phase-1 gray rhyolitic pumice, here referred to as the Millennium gray pumice, to the less-explosive phase-2 black trachytic pumice^{12,14} (Fig. 1). The pumice samples analyzed for this study are the alkali rhyolitic pumice collected from three proximal air-fall deposit sites on the rim of the summit caldera and from medial to distal PDC deposits north of Baekdusan (Fig. 1).

Results

Bubble pocket texture. The Millennium gray pumice contains an unusual vesicle structure referred to as bubble pockets. The bubble pockets are near-spherical clusters of bubbles ranging in diameter from a few millimeters to more than one centimeter. A reticular network of extremely thin (<10 μm) glass films fills the interior of bubble pockets and surrounds fractured alkali feldspar phenocrysts (Fig. 2). On three-dimensional X-ray tomographic sections, the bubble pockets appear as spherical voids (high X-ray penetrance owing to extremely high vesicularity) containing high-brightness (low X-ray penetrance) crystal fragments (Fig. 2b, c).



Maps Data: Google Earth Pro, CNES / Airbus Maxar Technologies Landsat / Copernicus

Fig. 1 Sampling locations and field photographs. **a** Satellite image showing the sampling locations (**b–g**). **b–d** Field photographs of the proximal Millennium pumice-fall deposits on the rim of the Cheonji caldera. **e–g** Outcrop photographs of the medial to distal PDC and/or lahar deposits of the Millennium pumice.

In contrast, the domain outside the pockets shows medium brightness (moderate X-ray penetrance) and tubular-stretched vesicle textures (Fig. 2c). The volume fraction of the bubble pockets exceeded 20% for three of the five pumice samples and was up to 24% for one sample (Fig. 3a).

Individual bubbles inside the pockets are subspherical, with diameters $>100\ \mu\text{m}$ and up to $>1000\ \mu\text{m}$ in some cases (Fig. 2d). In contrast, bubbles in the host domain are elliptical or elongated, with thicker and often composite bubble walls. All individual bubble pockets contain at least one phenocryst or glomerocryst, mainly sanidine or anorthoclase. These crystals are variably fragmented into pieces with jigsaw-fit margins (Fig. 2d). Feldspar fragments have numerous cavities filled with vesiculated glass inclusions (Fig. 2f). These cavities commonly have fracture-controlled openings as inclusion glass expands into foam, a typical feature of ruptured melt inclusions⁵. The vesicularity, calculated from the cross-sectional area of vesicles, ranged between 82.8% and 90.6% inside the bubble pockets and between 59.4% and 65.8% outside the bubble pockets (Fig. 3b).

Petrochemical characteristics of the Millennium gray pumice.

The Millennium gray pumice has a whole-rock composition of sodic rhyolite (comendite) and contains approximately 3 vol.% of

phenocrysts that are significantly lower than that of the upper black trachyte (10–20 vol.%)²³. The phenocryst content of the Millennium gray pumice mainly comprises K-feldspar, here classified into sanidine and anorthoclase, and includes very small amounts of quartz, plagioclase, fayalite and titanite¹². The pumice shows considerable heterogeneity in glass and feldspar compositions at the microscopic level (Fig. 4). The EPMA point analysis revealed that bubble pockets in Millennium gray pumice have two distinctive glass-alkali feldspar assemblages (Fig. 4). The two distinctive types of bubble pockets, namely type-A and type-B, and the host domain surrounding bubble pockets make a unique triple chemo-textural zonation pattern of the Millennium gray pumice.

The type-A bubble pockets (red domain in Fig. 4a) comprise trachytic (65–70 in SiO_2 wt.%) bubble-wall and remnant (but vesiculated) inclusion glasses (Fig. 4d), and fractured sanidine phenocrysts (Fig. 4e). In contrast, the type-B bubble pockets (yellow domain in Fig. 4a) contain a rhyolitic (73–75 in SiO_2 wt.%) bubble-wall and remnant inclusion glasses (Fig. 4d) and anorthoclase phenocrysts (Fig. 4e). The host domain (orange domain in Fig. 4a), lacking in feldspar phenocryst, has generally rhyolitic glass compositions, but it further covers intermediate realm toward trachyte (70–75 in SiO_2 wt.%) particularly near the type-A bubble pockets (Fig. 4d). The trachytic type-A bubble pockets are commonly larger in pocket diameter (mostly $>5\ \text{mm}$ and occasionally $>10\ \text{mm}$)

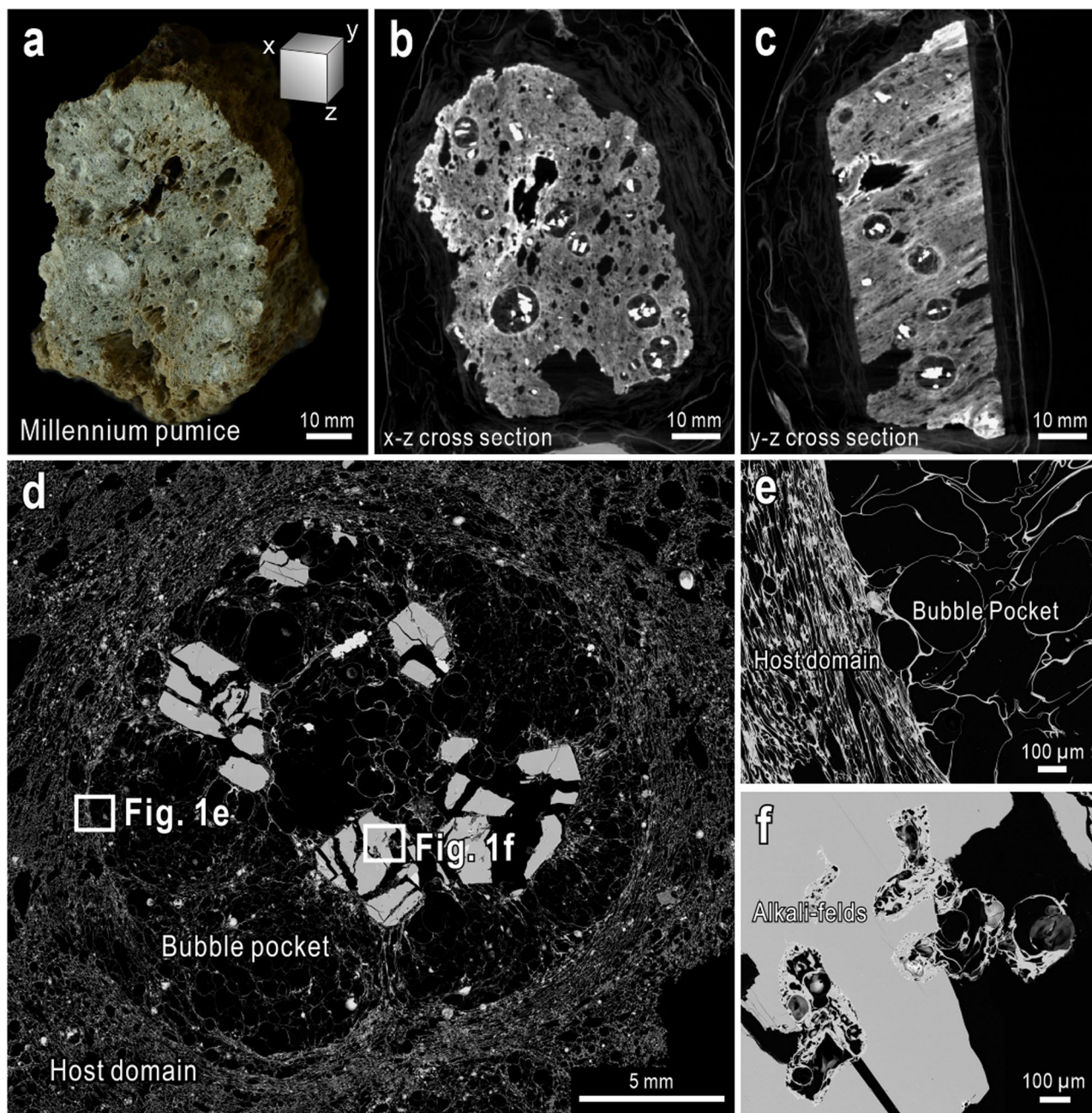


Fig. 2 Multi-scale cross-sectional images of the Millennium gray pumice. **a** Photograph of a pumice hand specimen. **b, c** Computerized tomographic sections normal and parallel to the elongation directions of vesicles, showing the 3D shape and population of bubble pockets and host foam in the Millennium gray pumice. **d** Merged SEM-BSE image showing details of bubbles, bubble walls and crystal fragments in- and outside of a bubble pocket. SEM-BSE images showing textural details of **e** gas bubbles near the boundary of the bubble pocket, and **f** vesiculated melt inclusions bursting out from cavities in fragmented K-feldspar phenocryst.

than the rhyolitic type-B bubble pockets (mostly <5 mm in diameter) and contain significantly larger (mostly >2 mm and occasionally >5 mm in the long axis) phenocrysts than the type-B pockets (mostly <2 mm in the long axis).

Discussion

Formation of bubble pockets. Fractured phenocrysts containing vesiculated glass inclusions are commonly found in pyroclastic deposits^{25–29}, and have been attributed to rupture and violent vesiculation (burst) of melt inclusions. The textural and petrochemical evidence, such as fragmented alkali feldspars and ruptured

inclusion glasses therein, suggests that the bubble pockets in the Millennium gray pumice were produced by the burst of melt inclusions formerly trapped in alkali feldspar phenocrysts in an already highly vesiculated and shear-strained host magma. The tubular-stretched vesicle texture outside the bubble pockets (host domain) indicates the extreme viscous shear deformation of bubble-rich magma ascending through a conduit during the climactic Plinian eruptive phase³⁰. In contrast, the fragmented sanidine/anorthoclase phenocrysts inside each bubble pocket (Fig. 2b, c) and the near-spherical bubble pockets indicate a single isotropic dilation of the bursting melt inclusions without further shear deformation. The lack of shear deformation implies that the burst of melt inclusions

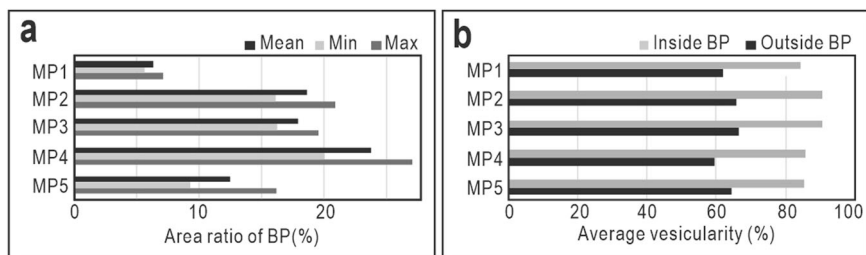


Fig. 3 Cross-sectional area ratio of five selected Millennium gray pumice samples. **a** The ratio of the area occupied by bubble pockets in CT sections. **b** Vesicularity approximated based on the area ratio analysis of gas bubbles in SEM-BSE images. CT and SEM-BSE images were analyzed using ImageJ™ image-analysis software. BP bubble pockets.

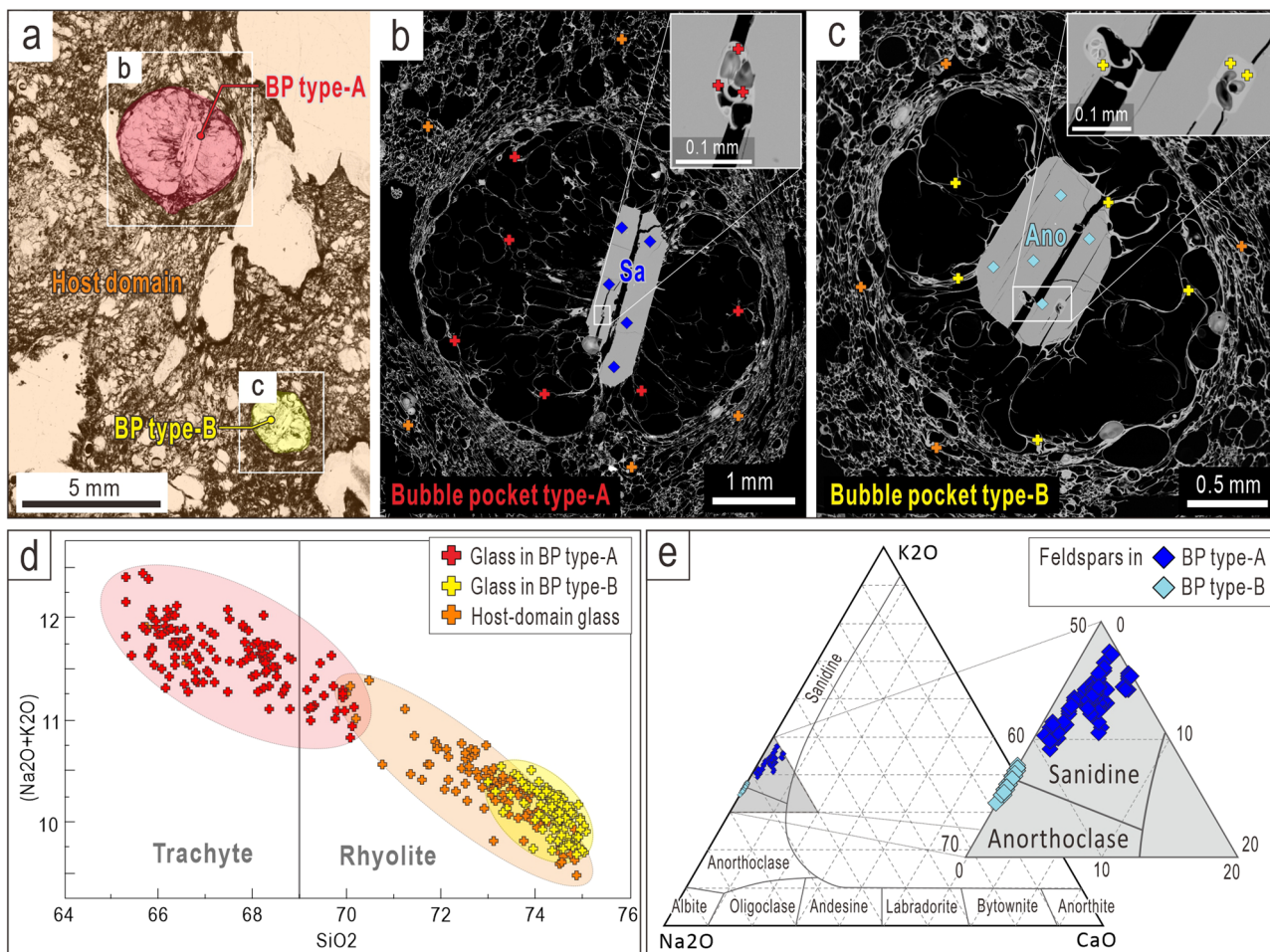


Fig. 4 Petrochemical characteristics of the Millennium gray pumice. **a** Scanned thin section and BSE images of bubble pockets type-A (**b**) and type-B (**c**). Crosses and diamonds represent the locations of EPMA point analyses on glasses and K-feldspars, respectively. For the information of colors, see the legends in Fig. 4d, e. **d** Total Alkali-Silica diagram showing the glass compositions of the three distinctive domains in the Millennium gray pumice. The red and yellow colors represent glass compositions in type-A and type-B bubble pockets, respectively. The orange color represents the host glass composition. **e** Ternary diagram showing the compositions of feldspars in different types of bubble pockets. The dark and light blue colors represent compositions of feldspars in type-A and type-B bubble pockets, respectively.

occurred when their host magma reached the fragmentation level, immediately before or more possibly at the moment of fragmentation. Rapid chilling preserved the fine wall textures within the bubble pockets. Post-eruptive rupture of the melt inclusions is unlikely, as bubble growth in such high-viscosity rhyolitic magmas is limited after eruption^{31,32}.

Heterogeneous vesicle textures were reported from pumice originating from c. 4.1 ka Agnano Monte Spina eruption at

Campi Flegrei³³, Italy, highly similar to the bubble pocket texture of the Millennium gray pumice. The Campi Flegrei pumice shows subspherical phenocryst-bearing (i.e., pyroxene, feldspar and biotite) vesicle pockets surrounded by stretched and eventually pinch-off vesicles. The case, however, does not involve rupture of melt inclusions, thereby regarded as a consequence of heterogeneous bubble nucleation or second boiling around micro-phenocrysts³³.

Magmatic control of the 946 CE Plinian eruption at Baekdusan. The two different types of bubble pockets coexisting within the chemically intermediate host domain of the Millennium gray pumice imply cryptic mixing between two different (rhyolite and trachyte) subvolcanic magmas, probably playing a critical role in driving the Millennium Eruption. Here, we suggest a four-step conceptual model of the inceptive cryptic magma mixing and subsequent simultaneous burst of melt inclusions that formed the unique triple chemo-textural domains within the Millennium gray pumice (Fig. 5).

The stratigraphic studies of the Baekdusan Volcano commonly reported a rhyolitic Plinian event at c. 50 ka BP (known as the TWF eruption) that deposited a thick pile of yellowish air-fall pumice right below the Millennium gray pumice (Pan et al.¹⁴ and references therein). The presence of TWF pumice infers that the system of repetitive fractionation and eruption of rhyolitic magma from its trachytic host was initiated far before the Holocene. Given the zircon U-Th ages of c. 12.2 ± 1.1 ka for the phase-1 comendite pumice (Millennium gray pumice) and c. 2.6 ± 1.8 ka for the phase-2 trachyte pumice¹⁷, it is inferred that the rhyolite magma that fed the Millennium Eruption began to accumulate at the final storage level far before the arrival of the trachyte magma. The Ra/Th isotope age model¹⁶ suggests that the trachyte magma accumulated from 2.5 to 1.5 ka BP right beneath but separated from the pre-existing rhyolite body with limited mixing.

It is generally accepted that the stable positions of the rhyolite and trachyte bodies were disrupted by the pulse of a more primitive trachyandesitic magma^{14,16}. In the Millennium gray pumice originating from the climactic phase of the Millennium Eruption, however, no evidence of the trachyandesitic melt association is found. This may imply that the trachyandesite magma played a limited role as a trigger of cryptic magma mixing and subvolcanic magma ascent. The disruption (or overturn) of rhyolite-trachyte magma assemblage by a new magma injection might have developed overpressure (through an increase of either magmatic volume or gas pressure)^{34,35}, which readily cracked open the roof of the subvolcanic reservoir and consequently initiated magma ascent for the 946 CE Plinian eruption (Step 1).

As the reservoir magma began to rise and accelerate through volcanic conduit, the initially separated trachyte and rhyolite bodies began to be mechanically mixed by shear (Step 2). The progressive intense mechanical shearing applied on the acceleratingly ascending conduit magma might have enabled the two highly viscous magmas to be physically mixed under chemical disequilibrium. The progressive mechanical mixing might have been maintained until the conduit magma reached the fragmentation level (Steps 3 and 4), above which the magma began to burst into pumice fragments. The dominance of rhyolitic host glass relative to trachytic glass in the Millennium pumice (Fig. 4d) implies that the incorporated trachyte magma was volumetrically smaller than the rhyolite magma. In this stage, sanidine phenocrysts containing abundant trachytic melt inclusions were drawn into the anorthoclase-bearing rhyolite magma body. As decompression reached a critical level, saturated volatiles (mostly H₂O) began to spontaneously exsolve from the host melt and nucleate gas bubbles (Step 2).

Along with the continuous magma ascent, gas bubbles in the host melt progressively increased in size and population, and they attained tubular-stretched forms by shear (Steps 2–3). The increasing volume fraction of gas bubbles made the rising magma body more viscous but mechanically fragile and thus ultimately prone to fragmentation¹. As the magma approached the fragmentation level, both sanidine and anorthoclase phenocrysts began to rupture simultaneously (Step 3) owing to extreme decompression, shock wave, choked flow, and fragmentation

stresses^{7,28,36}. The simultaneous rupture of alkali feldspars allowed the volatile-supersaturated melt inclusions to suddenly reach the near-atmospheric pressure and initiate the second-stage bubble formation (Step 3).

The melt inclusions, preserving the original volatile contents, then violently burst out of fractured crystal seals and instantaneously expanded to form spherical domains (bubble pockets) approximately 20% more vesicular than the host domain (Step 4). We deduce that the catastrophic burst of melt inclusions resulted in additional pressurization, expansion, and structural instability of the fragmenting magma body, ultimately enhancing the efficiency of magma fragmentation and the explosivity of the 946 CE Plinian eruption at Baekdusan. The highly variable volume fractions (6–24%) of the bubble pockets among the Millennium gray pumice samples reflect incomplete cryptic magma mixing. Despite this heterogeneity, the impact of second-stage bubble formation on the erupting magma body appears to have been significant.

Glass shard heterogeneity in the B-Tm tephra. The B-Tm tephra, the distal ash-fall layers coeval with the proximal Millennium pumice, is one of the most intensively studied time marker of the northern hemisphere. One of the distinctive features of the B-Tm tephra is its transitional glass shard composition between trachyte and rhyolite endmembers, recognized by numerous studies on variable locations of northern Japanese Island and the East Sea (Japan Sea) regions^{11,13,15,24,37–40}. Researchers regarded the compositional continuum found in B-Tm tephra as strong evidence pointing toward the mixing of two compositionally distinct magma batches during the Millennium Eruption^{12,37}. However, such intermediate glass compositions have not yet been reported in the proximal records³⁷, and thus some attributed compositional heterogeneity of the B-Tm tephra to the mixing of trachytic and rhyolitic glass shards originating from different phases (rhyolitic phase-1 and trachytic phase-2) of the Millennium Eruption^{13–15}.

The triple chemo-textural zonation pattern first reported in this study provides the missing link between the proximal Millennium pumice and distal B-Tm tephra. The two endmember bubble pocket glasses and the intermediate host glass, coexisting within almost every single Millennium gray pumice, evince that the compositional heterogeneity of the B-Tm tephra did not necessarily involve sedimentological mixing between ashes from different eruptive phases, but is a feature of the cryptically mixed source magma that fed the early climactic phase of the Millennium Eruption. We infer that the second trachytic phase of the Millennium Eruption was less explosive than the first climactic Plinian phase, thus, unlikely to have contributed to the formation of the distal B-Tm tephra. In conclusion, we suggest that the B-Tm tephra does not represent the whole eruptive phases of the Millennium Eruption but is only a product of the earlier climactic Plinian phase fed by a cryptically mixed source magma.

Conclusions

We have investigated the chemo-textural character of the Millennium gray pumice and drawn the following conclusions.

1. The earlier phase of the 946 CE Plinian eruption at Baekdusan was driven by cryptic magma mixing and simultaneous burst of melt inclusions as evidenced by the three distinctive chemo-textural domains (bubble pockets type-A and type-B and the host domain) within the Millennium gray pumice.
2. The simultaneous bursting of melt inclusions increased the volume of magma by about 6–24% near the magma

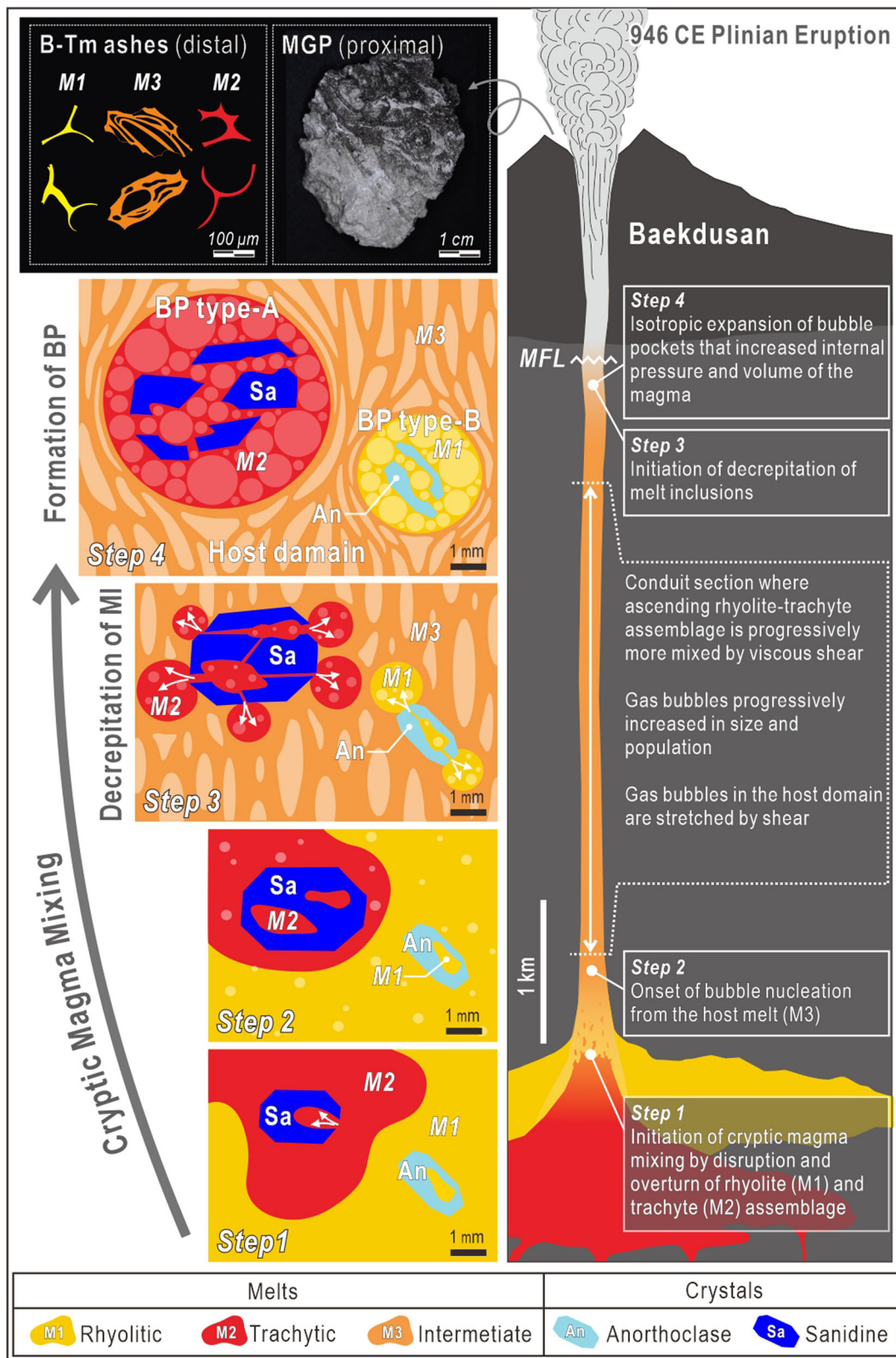


Fig. 5 Schematics of the volcanic plumbing system during the 946 CE Millennium Eruption at Baekdusan. The model conceptualizes the cryptic magma mixing and formative process of bubble pockets during the Millennium Eruption. MGP Millennium gray pumice, BP bubble pocket, M melt inclusion, MFL magma fragmentation level.

fragmentation level. The volume change of the magma probably contributed to increasing the eruption rate and exit velocity of tephra from the vent, thereby enhancing the overall explosivity of the 946 CE Plinian eruption at Baekdusan.

- The chemically heterogeneous glass shards of the distal B-Tm tephra might have originated from the three chemically distinctive domains of cryptically mixed magma that fed the 946 CE Plinian eruption at Baekdusan.

The bubble pocket texture reported here may be a common but overlooked feature of pumice generated by explosive silicic volcanism. The excess explosivity induced by the burst of melt inclusions at the final moment of magma fragmentation seems to be an important process that needs to be taken into account when modeling the eruption dynamics and assessing volcanic hazards. Further investigation into the diversity of bubble pocket textures from multiple volcanoes may help understand the variations in eruption styles and intensities of silicic volcanoes.

Methods

The vesicle structures of five randomly selected pumice hand specimens (5–20 cm in the long axis) were investigated using a computerized X-ray tomography (CT) machine at the Korea Institute of Geoscience and Mineral Resources. The machine is equipped with two switchable X-ray tubes of 225 and 160 kV, one flat panel detector with 2048 × 2048 pixels (optional binning possible) and one rotary stage of 36 arcsec (~0.001°) resolution. The CT scanning was conducted at an operating voltage of 90 kV and current of 70 μm with a rotation angle of 0.5° and exposure time of 2 s. The distances from source to object and object to detector were set at 269.602 and 588.488 mm, respectively. Owing to the low CT image resolution (0.126 mm), the micro-textures of glass bubble walls and phenocrysts of pumice were investigated based on back-scattered electron (BSE) imaging of polished sections. The volume fraction of bubble pockets and vesicularity of pumice samples were calculated using CT and BSE images loaded on the open-source image-analysis program IMAGEJ™ (<https://imagej.net>) (Supplementary Fig. 1, Supplementary Data 1; Kim et al.⁴¹). To prevent the destruction of delicate glass bubble walls, rectangular parallelepiped chips of pumice samples were vacuum impregnated with Epofix™ resin prior to the polished section making.

The chemical compositions of the glass and feldspar phenocrysts were determined at Gyeongsang National University using an electron probe microanalysis (EPMA, JEOL JXA-8530F) equipped with five wavelength-dispersive X-ray spectrometers (Supplementary Data 2). The instrument was operated at an accelerating voltage of 15 kV and currents ranging between 5 and 10 nA, depending on the beam diameters (10, 15, or 20 μm). Standards supplied by JEOL were used for the analysis of major elements. Diopside was used for Mg and Si; K-feldspar for K; kyanite for Al; albite for Na; ilmenite for Fe and Ti; garnet for Mn; wollastonite for Ca; and synthetic InP for P. To prevent alkali loss, glass parts in pumice were analyzed with counting times of 5 s for Na and K and 10 s for the other elements. Each background signal was counted at half the time of the peak. A secondary glass standard, 81003G from Erebus Volcano (Kelly et al.⁴²), was used for the precise EPMA calibration.

Data availability

The volume fractions and petrochemical data sets used to analyze the physical and chemical properties of the Millennium gray pumice can be accessed via Figshare (<https://doi.org/10.6084/m9.figshare.23925669>).

Received: 2 March 2023; Accepted: 8 September 2023;

Published online: 16 September 2023

References

- Schmincke, H. U. *Volcanism* Vol. 28 (Springer Science & Business Media, 2004).
- Cluzel, N., Laporte, D., Provost, A. & Kannevischer, I. Kinetics of heterogeneous bubble nucleation in rhyolitic melts: implications for the number density of bubbles in volcanic conduits and for pumice textures. *Contrib. Mineral. Petrol.* **156**, 745–763 (2008).
- Hurwitz, S. & Navon, O. Bubble nucleation in rhyolitic melts: experiments at high pressure, temperature, and water content. *Earth Planet. Sci. Lett.* **122**, 267–280 (1994).
- Tait, S. Selective preservation of melt inclusions in igneous phenocrysts. *Am. Min.* **77**, 146–155 (1992).
- Belkin, H. E. & De Vivo, B. Fluid inclusion studies of ejected nodules from plinian eruptions of Mt. Somma-Vesuvius. *J. Volcanol. Geotherm. Res.* **58**, 89–100 (1993).
- Blundy, J. & Cashman, K. Rapid decompression-driven crystallization recorded by melt inclusions from Mount St. Helens volcano. *Geology* **33**, 793–796 (2005).
- Maclennan, J. Bubble formation and decrepitation control the CO₂ content of olivine-hosted melt inclusions. *Geochem. Geophys. Geosystem* **18**, 597–616 (2017).
- Yang, Q. et al. The Millennium eruption of Changbaishan Tianchi Volcano is VEI 6, not 7. *Bull. Volcanol.* **83**, 1–10 (2021).
- Oppenheimer, C. et al. Multi-proxy dating the ‘Millennium Eruption’ of Changbaishan to late 946 CE. *Quat. Sci. Rev.* **158**, 164–171 (2017).
- Machida, H. The stratigraphy, chronology and distribution of distal marker-tephras in and around Japan. *Glob. Planet. Change* **21**, 71–94 (1999).
- McLean, D. et al. Identification of the Changbaishan ‘Millennium’ (B-Tm) eruption deposit in the Lake Suigetsu (SG06) sedimentary archive, Japan: synchronisation of hemispheric-wide palaeoclimate archives. *Quat. Sci. Rev.* **150**, 301–307 (2016).
- Sparks, R. S. J. et al. *Volcanic Plumes* (Wiley, 1997).
- Furuta, T., Fujioka, K. & Arai, F. Widespread submarine tephra around Japan—petrographic and chemical properties. *Mar. Geol.* **72**, 125–142 (1986).
- Pan, B. et al. The VEI-7 Millennium eruption, Changbaishan-Tianchi volcano, China/DPRK: new field, petrological, and chemical constraints on stratigraphy, volcanology, and magma dynamics. *J. Volcanol. Geotherm. Res.* **343**, 45–59 (2017).
- Tokui, Y. Volcanic eruptions and their effects on human activity, in Hokkaido, Japan. *Ann. Ochanomizu Geograph. Soc.* **30**, 27–33 (1989).
- Ramos, F. C. et al. U-series and 40Ar/39Ar ages of Holocene volcanic rocks at Changbaishan volcano, China. *Geology* **44**, 511–514 (2016).
- Zou, H., Fan, Q., Zhang, H. & Schmitt, A. K. U-series zircon age constraints on the plumbing system and magma residence times of the Changbai volcano, China/North Korea border. *Lithos* **200**, 169–180 (2014).
- Pappalardo, L. et al. The role of CO₂ flushing in triggering the ‘Millennium’ eruption and recent unrests at Changbaishan volcano (China/North Korea). *Int. Geol. Rev.* **65**, 706–719 (2023).
- Pan, B., de Silva, S. L., Xu, J., Liu, S. & Xu, D. Late Pleistocene to present day eruptive history of the Changbaishan-Tianchi Volcano, China/DPRK: new field, geochronological and chemical constraints. *J. Volcanol. Geotherm. Res.* **399**, 106870 (2020).
- Wei, H., Liu, G. & Gill, J. Review of eruptive activity at Tianchi volcano, Changbaishan, northeast China: implications for possible future eruptions. *Bull. Volcanol.* **75**, 1–14 (2013).
- Zhang, M. et al. The intraplate Changbaishan volcanic field (China/North Korea): a review on eruptive history, magma genesis, geodynamic significance, recent dynamics and potential hazards. *Earth-Sci. Rev.* **187**, 19–52 (2018).
- Dunlap, C. E. *Physical, Chemical, and Temporal Relations among Products of the 11th Century Eruption of Baitoushan, China/North Korea*. Doctoral dissertation, University of California Santa Cruz (1996).
- Horn, S. & Schmincke, H. U. Volatile emission during the eruption of Baitoushan Volcano (China/North Korea) ca. 969 AD. *Bull. Volcanol.* **61**, 537–555 (2000).
- Machida, H. The recent major eruption of Changbai Volcano and its environmental effects. *Geographical Reports of Tokyo Metropolitan University*, 1–20 (1990).
- Best, M. G. & Christiansen, E. H. Origin of broken phenocrysts in ash-flow tuffs. *Geol. Soc. Am. Bull.* **109**, 63–73 (1997).
- Gualda, G. A. & Anderson, A. T. Magnetite scavenging and the buoyancy of bubbles in magmas. Part 1: discovery of a pre-eruptive bubble in Bishop rhyolite. *Contrib. Mineral. Petrol.* **153**, 733–742 (2007).

27. Kennedy, B. et al. Conduit implosion during Vulcanian eruptions. *Geology* **33**, 581–584 (2005).
28. Miwa, T. & Geshi, N. Decompression rate of magma at fragmentation: inference from broken crystals in pumice of Vulcanian eruption. *J. Volcanol. Geotherm. Res.* **227**, 76–84 (2012).
29. Rotella, M. D. et al. Dynamics of deep submarine silicic explosive eruptions in the Kermadec arc, as reflected in pumice vesicularity textures. *J. Volcanol. Geotherm. Res.* **301**, 314–332 (2015).
30. Manga, M., Castro, J., Cashman, K. V. & Loewenberg, M. Rheology of bubble-bearing magmas. *J. Volcanol. Geotherm. Res.* **87**, 15–28 (1998).
31. Gardner, J. E., Carey, S., Sigurdsson, H. & Rutherford, M. J. Influence of magma composition on the eruptive activity of Mount St. Helens, Washington. *Geology* **23**, 523–526 (1995).
32. Klug, C. & Cashman, K. V. Permeability development in vesiculating magmas: implications for fragmentation. *Bull. Volcanol.* **58**, 87–100 (1996).
33. Piochi, M., Polacci, M., Arzilli, F. & Ventura, G. Microscale textural heterogeneity and tip-streaming instability in alkaline magmas: evidence in tube pumices from Campi Flegrei, Italy. *J. Volcanol. Geotherm. Res.* **413**, 107200 (2021).
34. Cas, R. & Wright, J. *Volcanic Successions Modern and Ancient: A Geological Approach to Processes, Products and Successions* (Springer Science & Business Media, 2012).
35. Sun, C. et al. Ash from Changbaishan Millennium eruption recorded in Greenland ice: implications for determining the eruption's timing and impact. *Geophys. Res. Lett.* **41**, 694–701 (2014).
36. Bindeman, I. N. Fragmentation phenomena in populations of magmatic crystals. *Am. Min.* **90**, 1801–1815 (2005).
37. Chen, X. Y. et al. Clarifying the distal to proximal tephrochronology of the Millennium (B–Tm) eruption, Changbaishan Volcano, northeast China. *Quat. Geochronol.* **33**, 61–75 (2016).
38. Nanayama, F. et al. Unusually large earthquakes inferred from tsunami deposits along the Kuril trench. *Nature* **424**, 660–663 (2003).
39. Nara, F. W. et al. Characteristics in trace elements compositions of tephros (B–Tm and To-a) for identification tools. *Geochem. J.* **55**, 117–133 (2021).
40. Okuno, M. et al. Widespread tephros in sediments from lake Ichi-no-Megata in northern Japan: their description, correlation and significance. *Quat. Int.* **246**, 270–277 (2011).
41. Kim, G. B. et al. Supplementary data for COMMSENV-23-0268B. Figshare. Dataset <https://doi.org/10.6084/m9.figshare.23925669> (2023).
42. Kelly, P. J., Kyle, P. R., Dunbar, N. W. & Sims, K. W. Geochemistry and mineralogy of the phonolite lava lake, Erebus volcano, Antarctica: 1972–2004 and comparison with older lavas. *J. Volcanol. Geotherm. Res.* **177**, 589–605 (2008).

Acknowledgements

This study was supported by the National Research Foundation of Korea (NRF) grant funded by the Korean government (MSIT) (NRF-2018R1A1A1A05077465 and RS-2023-00209301). The Millennium gray pumice samples examined for this study were collected during the Korea–China joint research program in 2014 and 2015.

The collected pumice samples were transported to Gyeongsang National University, Republic of Korea, for analysis under the official permission and logistic support of the Chinese Academy of Sciences (CAS), China. We appreciate Korea Polar Research Institute (KOPRI) for analytical advice.

Author contributions

G.B.K. conceptualized the paper and conducted experimental analysis and paper writing. Y.K.S. contributed to project administration, conceptualization and paper writing. S.J.C. independently cross-checked the petrochemical data sets and conceptualized the cryptic magma mixing. J.O.J. operated EPMA analysis and checked the quality of petrochemical data. S.Y.G. supported graphic analysis of CT and SEM-BSE images. Y.S.L. and J.L. organized the Korea–China joint research and provided logistic support. All authors supported the writing and editing process.

Competing interests

The authors declare no competing interests.

Additional information

Supplementary information The online version contains supplementary material available at <https://doi.org/10.1038/s43247-023-00995-z>.

Correspondence and requests for materials should be addressed to Young Kwan Sohn.

Peer review information *Communications Earth & Environment* thanks Barbara Bonechi, Fabio Arzilli and the other, anonymous, reviewer(s) for their contribution to the peer review of this work. Primary Handling Editor: Joe Aslin. A peer review file is available.

Reprints and permission information is available at <http://www.nature.com/reprints>

Publisher's note Springer Nature remains neutral with regard to jurisdictional claims in published maps and institutional affiliations.



Open Access This article is licensed under a Creative Commons Attribution 4.0 International License, which permits use, sharing, adaptation, distribution and reproduction in any medium or format, as long as you give appropriate credit to the original author(s) and the source, provide a link to the Creative Commons licence, and indicate if changes were made. The images or other third party material in this article are included in the article's Creative Commons licence, unless indicated otherwise in a credit line to the material. If material is not included in the article's Creative Commons licence and your intended use is not permitted by statutory regulation or exceeds the permitted use, you will need to obtain permission directly from the copyright holder. To view a copy of this licence, visit <http://creativecommons.org/licenses/by/4.0/>.

© The Author(s) 2023